Electronic Factors Affecting Second-Order NLO Properties: Case Study of Four Different Push-Pull Bis-Dithiolene Nickel Complexes

ARTICLE *in* INORGANIC CHEMISTRY · SEPTEMBER 2004

Impact Factor: 4.76 · DOI: 10.1021/ic0496469 · Source: PubMed

Inorg. Chem. **2004**, *43*, 5069–5079

Electronic Factors Affecting Second-Order NLO Properties: Case Study of Four Different Push-Pull Bis-Dithiolene Nickel Complexes

Simona Curreli,[†] Paola Deplano,*[,†] Christophe Faulmann,[‡] Andrea Ienco,[§] Carlo Mealli,*[,§] Maria Laura Mercuri,[†] Luca Pilia,[†] Gloria Pintus,[†] Angela Serpe,[†] and Emanuele F. Trogu[†]

Dipartimento di Chimica Inorganica ed Analitica, Università di Cagliari, I-09042 Monserrato (Cagliari) Italy, LCC-CNRS, 205, Route de Narbonne, 31077 Toulouse Cedex 04, France, and ICCOM-CNR, via Madonna del Piano, I-50019 Sesto Fiorentino (Firenze), Italy

Received March 17, 2004

The paper presents a detailed experimental and theoretical study of the four mixed nickel–bisdithiolene complexes [Ni(Pr^i_2pipdt)(dmit)] (**1b**, Pr^i_2pipdt = 1,4-diisopropyl-piperazine-3,2-dithione; dmit = 1,3-dithiolo-2-tione-4,5-dithiolato), [Ni(R_2pipdt)(mnt)] (**2b′′**, R = 2-ethylhexyl; mnt = maleonitriledithiolato), [Ni(Pr^i_2timdt)(dmit)] (**3b**, Pr^i_2timdt = 1,3-diisopropyl-imidazoline-2,4,5-trithione), and [Ni(Pr^i_2timdt)(mnt)] (**4b**), and their models. All the complexes, with common $(C_2S_2)Ni(C_2S_2)$ core and two different terminal groups, are uncharged and square-planar coordinated. Previous measurements of the first molecular hyperpolarizability indicated that some of the species are potential NLO chromophores due to the π-delocalized character of two frontier levels (HOMO and LUMO) which is asymmetrically perturbed by the combination of one *push* (R_2pipdt, R_2timdt) with one *pull* ligand (dmit and mnt). The X-ray structure of complex **1b** is presented and its geometry is compared with those available in the literature for the four types of complexes under study. The results of electrochemical and spectroscopic measurements (oxidation and reduction potentials, IR, dipole moment, molecular absorptivities, etc.) indicate rather different responses between the pairs of complexes **1**–**2** and **3**–**4**. Hence, DFT calculations on the model compounds **1a**–**4a**, where hydrogen atoms replace the alkyl groups of R_2pipdt and R_2timdt, have been carried out to correlate geometries and electronic structures. Moreover, the first molecular hyperpolarizabilities have been calculated and their components have been analyzed with the simplest two-level approximation. The derived picture highlights the different roles of the two *push* and *pull* ligands, but also the peculiar perturbation of the π-electron density induced by the terminal CS_3 grouping of the ligand dmit.

Introduction

The interest toward metal bis-dithiolene complexes is related to their applications in the areas of conducting[1] and magnetic[2] molecular materials and also to their relevant optical properties.[3,4] Complexes with third-order optical and optical-limiting properties are still under intensive investigation.[3,4] The Mueller−Westerhoff pioneering work has shown that bis-dithiolene uncharged and planar complexes of the triad Ni, Pd, and Pt can be useful as near-infrared dyes for Q-switching the Nd:YAG lasers.[5] The electronic properties depend most likely on the distribution of the 14 π electrons in the $(C_2S_2)_2Ni$ core (four of them belonging to the metal). In symmetric complexes (R = R′ in Scheme 1), the overall π electron delocalization (form B) implies the equivalence

* Authors to whom correspondence should be addressed. E-mail: deplano@unica.it (P.D.); mealli@iccom.cnr.it (C.M.).
† Università di Cagliari.
‡ LCC-CNRS.
§ ICCOM-CNR.

(1) Stiefel, E. I., Ed. *Dithiolene Chemistry*; Progress in Inorganic Chemistry, Vol. 52; John Wiley & Sons: New York, 2004. Tanaka, H.; Okano, Y.; Kobayashi, H.; Suzuki, W.; Kobayashi, A. *Science* **2001**, *291*, 285.
(2) Coomber, A. T.; Beljonne, D.; Friend, R. H.; Brédas, J. K.; Charlton, A.; Robertson, N.; Underhill, A. E.; Kurmoo, M.; Day, P. *Nature* **1996**, *380*, 144. Robertson, N.; Cronin, L. *Coord. Chem. Rev.* **2002**, *227*, 93.
(3) Coe, B. J. In *Comprehensive Coordination Chemistry II*; McCleverty, J. A., Meyer T. J., Eds.; Elsevier-Pergamon: Boston, MA, 2004, Vol. 9.
(4) Tan, W. L.; Ji, W.; Zuo, J. L.; Bai, J. F.; You, X. Z.; Lim, Y. H.; Yang, S.; Hagan, D. J.; Van Stryland, E. W. *Appl. Phys.* **2000**, *B70*, 809.
(5) Mueller-Westerhoff, U. T. *Comprehensive Coordination Chemistry*; Wilkinson, G., Ed.; Pergamon Press: Oxford, 1987.

10.1021/ic0496469 CCC: $27.50
Published on Web 07/13/2004

Scheme 1

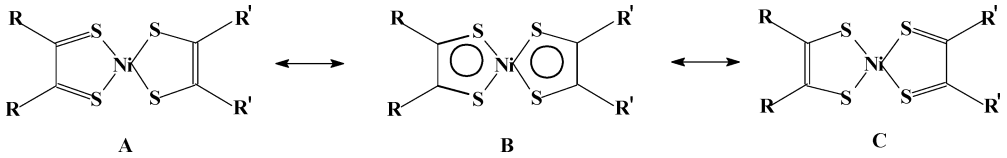

Scheme 2

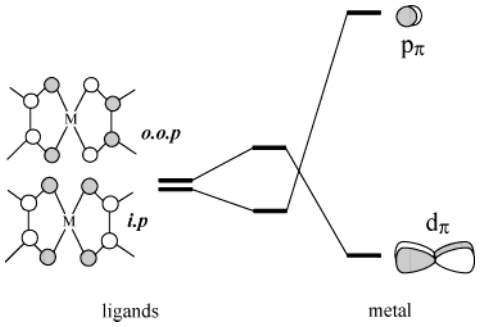

Scheme 3

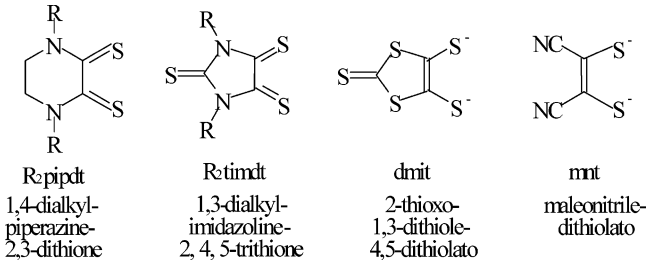

Scheme 4

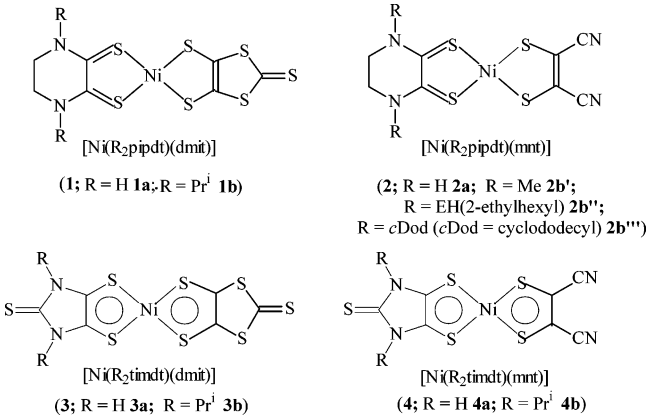

of resonance structures A and C. Conversely, different terminal groups attached to the core ($R \neq R'$) may cause a redistribution of the π electrons toward one of the limiting forms, A or C.[6]

Importantly, the nature of the substituents determines the stabilization of various ML_2 redox derivatives with charge spanning the range $+2/-2$. The latter limits are due to the fairly isolated frontier π MOs, which can be either empty or populated. As shown in Scheme 2, the *in-phase* (***ip***) and *out-of-phase* (***oop***) combinations of a C_2S_2 orbital (with C−C π and C−S π^* character) are stabilized and destabilized by one high lying p_π and a lower d_π orbital, respectively. For a stable and uncharged diamagnetic complex, only the lower MO is populated and the HOMO−LUMO gap is sufficiently large.[7]

In general, C_2S_2 π donor substituents (*push*) in symmetric complexes raise the energy of both the HOMO and the LUMO so that also the former is preferentially depopulated (cationic complexes). In contrast, π-acceptor substituents (*pull*) lower the energy of both the MOs and favor the dianionic state. The electronic effects of various substituents have been quantified for symmetric Ni, Pd, and Pt complexes.[6d]

In this paper, we consider four mixed nickel complexes that result from possible combinations of the four ligands depicted in Scheme 3. These carry either two terminal substituents (e.g., CN in mnt) or a condensed heterocycle over the C_2S_2 moiety (R_2pipdt, R_2timdt, and dmit, R = alkyl group). Some of these species have been theoretically analyzed by other authors.[8] Here, we will address how the different terminal environments (π-conjugated with the centrosymmetric $(C_2S_2)Ni(C_2S_2)$ core) can affect the electronic and the NLO properties of uncharged mixed complexes.

Interestingly, the symmetric ML_2 complexes, which are most readily synthesized with any of the mentioned ligands (M = group 10 metal), have different charges, i.e. they are dianionic (L = mnt), monoanionic (L = dmit), neutral (L = R_2timdt), and dicationic (L = R_2pipdt). Although all the species have a rich redox chemistry, the nature of their most accessible status is indicative of the basic *push* or *pull* character of the ligand. Thus, R_2pipdt and mnt are most evidently *push* and *pull*, respectively, and also dmit may be considered *pull*. However, the character is less evident when two S atoms of the terminal CS_3 moiety in the latter ligand are replaced by isoelectronic NH groupings (ligand R_2timdt). Thus, one goal of this study is that of evaluating the subtle differences in the electronic effects.

Four types of mixed and uncharged complexes are presented in Scheme 4 with different localized or delocalized descriptions, which can be corroborated also from the associated optical and spectroscopic properties. As proposed by Vogler in the early 1980s,[9] *asymmetric* bis-dithiolene complexes are potential second-order chromophores due to

(6) (a) Herman, Z. S.; Kirchner, R. F.; Loew, G. H.; Mueller-Westerhoff, U. T.; Nazal, A.; Zerner, M. C. *Inorg. Chem.* **1982**, *21*, 46. (b) Weber, J.; Daul, C.; Van Zelewsky, A.; Goursot, A.; Penigault, E. *Chem. Phys. Lett.* **1982**, *88*, 78. (c) Lauterbach, C.; Fabian, J. *Eur. J. Inorg. Chem.* **1999**, 1995. (d) Aragoni, C.; Arca, M.; Demartin, F.; Devillanova, F. A.; Garau, A.; Isaia, F.; Lelj, F.; Lippolis, V.; Verani, G. *J. Am. Chem. Soc.* **1999**, *121*, 7098.

(7) As an alternative viewpoint, the complex could feature singlet diradical ligands, as recently pointed out by some authors. However, while this is plausible for nitrogen analogues of the dithiolate ligands, the same authors consider negligible the diradical character in bis(*o*-benzodithiolate) nickel complexes. Bachler, V.; Olbrich, G.; Neese, F.; Wieghardt, K. *Inorg. Chem.* **2002**, *41*, 4179.

(8) Romaniello, P.; Lelj, F. *Chem. Phys. Lett.* **2003**, *372*, 51.

the inter-ligand charge-transfer character (CT) of the HOMO−LUMO transition[10] and most often they exhibit molecular first hyperpolarizability (β). Indeed, among the scarce examples of asymmetrical dithiolenes complexes,[9−11] some nickel ones have been experimentally found (by us[12] and others[13]) to exhibit second-order NLO properties.

Based on the measurements available, the complex [Ni(R$_2$pipdt)(mnt)], with R = 2-ethylhexyl (**2b″** in Scheme 4) associates a large ground-state dipole moment (μ_g = 16D) to negative solvatochromism ($\beta_o = -37 \times 10^{-30}$esu). The latter magnitude is even more pronounced in the complex [Ni(Pr$^i_2$pipdt)(dmit)], **1b**, ($\beta_o = -130 \times 10^{-30}$esu) while the μ_g value is slightly smaller (13D). In both cases, it may be assumed that the dithione−dithiolato structure (type **A**, in Scheme 1) is prevailing and that the dipole moment is directed from Pr$^i_2$pipdt toward the *pull* ligand (mnt or dmit). Upon the CT transition (excited state), the separation of charges could be quenched or even inverted. According to the typical two-level eq 1 (to estimate the first molecular hyperpolarizability from the lowest optically allowed HOMO−LUMO excitation),[14] the negative sign of β_{CT} depends only on $\mu_e < \mu_g$, with the other parameters (dipole transition moment, μ_{ge}, and energy gap, ΔE_{ge}) being both squared. Similar aspects were underlined also for the [M(diimine)(dithiolate)] complexes (M = Ni, Pd, Pt) investigated by the Eisenberg's group and others.[15,16]

$$\beta_{CT} \propto \frac{\mu_{ge}^{\ 2}\,\Delta\mu}{(\Delta E_{ge})^2} \qquad (1)$$

A different response is observed when the two NR groups adjacent to the C_2S_2 are inserted in five- rather than six-membered rings (R$_2$timdt vs. R$_2$pipdt). In fact, an almost null β_{CT} value has been measured for the complex [Ni(Pr$^i_2$timdt)(mnt)], **4b**, although the absence of NLO properties is accompanied by a large dipole moment (experimental μ_g value = 16 D).[12] Analogous data for [Ni(Pr$^i_2$timdt)(dmit)], **3b**, could better highlight the effect of the ligand Pr$^i_2$timdt but no solvatochromic measurement could be performed due to the insolubility of the species in any polar solvents.

This paper presents a detailed comparison of spectroscopic and structural data for compounds **1**−**4** as obtained from experiments and DFT calculations. In particular, we report the first X-ray characterization of a type **1** nickel complex, while the structures of type **4** remain undetermined due to the lack of suitable crystals. Also, the comparisons between the experimental and computed first molecular hyperpolarizabilities help to highlight the factors that influence the presence or absence of NLO properties.

Experimental Section

[Ni(Pr$^i_2$pipdt)(dmit)]. Crystals suitable for the diffractometric study were obtained by following a previously reported method which has been modified as follows.[12] (Bu$_4$N)$_2$[Ni(dmit)$_2$] (135 mg, 0.144 mmol) in 50 mL of THF, green solution, was added dropwise to [Ni(Pr$^i_2$pipdt)$_2$](BF$_4$)$_2$ (100 mg, 0.144 mmol) in 50 mL of CH$_3$CN, blue solution, at 50 °C under stirring. The solution became dark green and after 15 min warming and stirring were stopped. On slow evaporation of the solvents, green crystals precipitated. After one week these crystals were collected and washed with CH$_3$CN/THF, Et$_2$O in a 75% yield. Analytical results are in accordance with the formula [Ni(Pr$^i_2$pipdt)(dmit)]. Anal. Calcd for $C_{13}H_{18}N_2NiS_7$: C, 32.16; H, 3.74; N, 5.77; S, 46.02. Found: C, 32.20; H, 3.78; N, 5.80; S, 45.92. IR [cm^{-1}, KBr pellets] 2966 vw; 1492 vs; 1465 m; 1434 m; 1384 w; 1367 m; 1350 vs; 1285 vw; 1252 w; 1227 m; 1189 m; 1170 w; 1127 m; 1107 m; 1082 m; 1046 s; 1026 s; 967 w; 924 vw; 897 vw; 773 vw; 730 vw; 658 w; 600 vw; 593 vw; 515 w; 505 w; 475 m; 438 vw. Raman spectra (cm^{-1}) 1494 w; 1440 ms; 1351 w; 1278 w; 1223 vs; 1119 w; 1088 w; 923 w; 902 w; 877 vw; 518 m; 492 w; 472 w; 354 vs.

Spectroscopic Measurements. Microanalyses were performed by means of a Carlo Erba CHNS elemental analyzer model EA1108. IR spectra (4000−350 cm^{-1}) were recorded on a Bruker IFS55 FT-IR Spectrometer as KBr pellets. Raman spectra were carried out at room temperature on single crystals using a LABRAM-Jobin Yvon spectrometer equipped with an integrated microscope (BX 40, Olimpus) for micro Raman measurements. The excitation wavelength was a He−Ne (632.8 nm, 20 mW) laser, with the laser power being reduced by a factor of 100 to avoid sample damage and degradation. A 100× Objective has been used for the injection of laser line and collection of Raman signal in backscattering configuration. The laser line is removed by a holographic super notch filter and the Raman signal is dispersed by a stigmatic 300-mm focal length spectrometer equipped with two exchangeable gratings. An 1800 g/mm grating has been used to obtain the maximum in terms of spectral resolution (2.5 cm^{-1}). The signal is finally detected with CCD 1024 × 256 pixels cooled by a TE Peltier. The scattering peaks were calibrated against a Si standard (ν = 520 cm^{-1}). A typical spectrum was collected with a 500-s time constant and was averaged over 5 scans. No sample decomposition was observed during the experiments. Electronic spectra were recorded with a Cary 5 spectrophotometer. Cyclic voltammograms were carried out on a EG&G (Princeton Applied Research) potentiostat−galvanostat model 273, by using a conventional three-electrode cell consisting of a platinum wire working electrode, a platinum wire as counter-electrode, and Ag/AgCl in saturated KCl solution as reference electrode. The experiments were performed at room temperature (25 °C), in dry and argon-degassed CH$_3$CN containing 0.1 mol dm^{-3} Bu$_4$NPF$_6$ as supporting electrolyte, at 50−200 mV s^{-1} scan rate. Half-wave potential for ferrocene/ferrocenium couple (internal standard) is 0.43 V under the above conditions.

Data Collection and Structure Determination of 1b. The data were collected on a Stoe imaging plate diffraction system (IPDS) equipped with an Oxford Cryosystems cooler device. The crystal-to-detector distance was 70 mm, 161 exposures (3.5 min per exposure) were obtained with $0 < \phi < 225°$ and with the crystals rotated through 1.4° in ϕ. Crystal decay was monitored by measuring a maximum of 200 reflections per image. Cell parameters

(9) Vogler, A.; Kunkely, H. *Angew. Chem., Int. Ed. Eng.* **1982**, *21*, 77.
(10) Kato, R.; Kashimura, Y.; Sawa, H.; Okano, Y. *Chem. Lett.* **1997**, 921.
(11) Miller, T. R.; Dance, I. G. *J. Am. Chem. Soc.* **1973**, *95*, 6970.
(12) Bigoli, F. Chen, C.-T.; Deplano, P.; Mercuri, M. L.; Pellinghelli, M. A.; Pilia, L.; Pintus, G.; Serpe, A.; Trogu, E. F. *Chem. Commun.* **2001**, 2246.
(13) Chen, C.-T.; Liao, S.-Y.; Lin, K.-J.; Lai, L.-L. *Adv. Mater.* **1998**, *3*, 335.
(14) Kanis, D. R.; Ratner, M. A.; Marks, T. J. *Chem. Rev.* **1994**, *94*, 195, and references therein.
(15) Cummings, S. D.; Cheng, L.-T.; Eisenberg, R. *Chem. Mater.* **1997**, *9*, 440.
(16) Chen, C.-T.; Liao, S.-Y.; Lin, K.-J.; Chen, C.-H.; Lin, T.-Y J. *Inorg. Chem.* **1999**, *38*, 2734.

Table 1. Crystallographic Data of Compound [Ni(Pr$^i_2$pipdt)(dmit)], **1b**

	[Ni(Pr$^i_2$pipdt)(dmit)]
chemical formula	$C_{13}H_{18}N_2NiS_7$
fw	485.42
space group	$P2_1/n$ (No. 14)
a (Å)	10.3775(10)
b (Å)	16.1913(12)
c (Å)	12.2664(13)
β (deg)	109.893(11)
V (Å^3)	1938.1(3)
Z	4
T (K)	180
λ(Mo Kα) (Å)	0.71073
D_{calcd} (g/cm^3)	1.664
μ (cm^{-1})	17.53
R1 [$I > 2\sigma(I)$][a]	0.0277
wR2 (all data)[b]	0.0662

[a] $R1 = \sum | |F_o| - |F_c| | / \sum |F_o|$. [b] $wR2 = \{\sum [w(F_o^2 - F_c^2)^2] / \sum [w(F_o^2)^2]\}^{1/2}$.

were obtained from 8000 reflections taken from the data measurements between 2 and 26°. Crystal data and data collection details are presented in Table 1.

The structure was solved by using direct methods (Sir97[17]) and later refined by full-matrix least-squares methods on F^2 (Shelxl97[18]). The calculations were carried out with the WINGX[19] programs package running on a PC. An absorption correction based on the multiscan method[20] was applied to the data set. The hydrogen atoms were introduced at their ideal positions and all of their parameters were refined. The structural drawings were generated by using the programs ORTEP[21] and CAMERON.[22] The atomic scattering factors were taken from the international tables for X-ray crystallography.[23]

Computational Details. The structural optimizations were carried out at the hybrid density functional theory (DFT), by using the Becke's three-parameter hybrid exchange−correlation functional[24] with the nonlocal gradient correction of Lee, Yang, and Parr (B3LYP).[25] For this task, the program Gaussian98 was used.[26] The nature of all optimized structures were confirmed by calculations of the frequencies. A collection of Cartesian coordinates and total energies for all of the optimized molecules is available from the authors upon request. The basis set for nickel utilized the effective core potentials of Hay and Wadt[27] with the associated double-ζ valence basis functions. The basis set used for the remaining atomic species was the 6-31+G(d, p).[28]

The hyperpolarizability values were estimated by using the time-dependent extension of the density functional theory.[29] The calculations were performed with the ADF−RESPONSE module,[30] an extension of the Amsterdam Density Functional (ADF) package[31] running on the IBM SP4 cluster computer at CINECA supercomputer center. Single point calculations, by using the generalized gradient approximated potential (GGA) of Van Leeuwen and Baerends[32] (LB94), were performed with the molecular geometries previously optimized by Gaussian98. We used the ADF[33] triple ζ STO basis set with one 3d polarization function for C, N, S atoms and one 2p polarization function for H atom, and a triple ζ nd, (n + 1)s basis with one f type polarization function and one diffuse function. The cores 1s for C, N atoms, up to 2p for S and Ni atoms, were kept frozen.

To gain an overview of the major interactions between the $(C_2S_2)_2$Ni core and the terminal moieties, fragment orbital analyses were carried out by performing EHMO calculations[34] and the graphical analysis of the results with the package CACAO.[35] The geometries, optimized earlier with the DFT method, were used for this type of analysis. The goodness of the qualitative picture is supported by the consistent MO energy distribution and the level composition.

Results and Discussion

Synthesis and X-ray Structural Determination of [Ni(Pr$^i_2$pipdt)(dmit)], 1b. Well-formed green crystals of **1b** were obtained, as described in the Experimental Section, with a convenient method that allows preparation of several uncharged and asymmetric Ni-dithiolene complexes in high yields.[12] The method consists of reacting a symmetric nickel-dithiolene dication with a symmetric nickel-dithiolate dianion. In this case, a THF solution of $[Ni(Pr^i_2pipdt)_2](BF_4)_2$ was added dropwise to a CH_3CN solution of $(Bu_4N)_2[Ni(dmit)_2]$. On slow evaporation of the solvents, well formed green crystals precipitated. These crystals were characterized by X-ray structural analysis. Based on the knowledge of the space group ($P2_1/n$, centrosymmetric), no second-order NLO activity for crystals of **1b** is expected.

(17) Altomare, A.; Burla, M. C.; Cavalli, M.; Cascarano, G. L.; Giacovazzo, C.; Gagliardi, A.; Moliterni, A. G. G.; Polidori, G.; Spagna, R. *J. Appl. Crystallogr*. **1999**, *32*, 115−119.
(18) Sheldrick, G. M. Institüt für Anorganische Chemie der Universität, Tammanstrasse 4, D-3400 Göttingen, Germany, 1997.
(19) Farrugia, L. J. *J. Appl. Crystallogr*. **1999**, *32*, 837−838.
(20) Blessing, R. H. *Acta Crystallogr*., *Sect. A: Found. Crystallogr*. **1995**, *51*, 33−38.
(21) (a) ORTEP-III. Burnett, M. N., Johnson, C. K. *Report ORNL- 6895*; Oak Ridge National Laboratory: Oak Ridge, TN, 1996. (b) Farrugia, L. J. *J. Appl. Chem.* **1997**, *30*, 565. Farrugia, L. J. *J. Appl. Chem.* **1999**, *32*, 837.
(22) Watkin, D. J.; Prout, C. K.; Pearce, L. J. *CAMERON;* Chemical Crystallography Laboratory, University of Oxford, Oxford, U. K., 1996.
(23) Cromer, D. T.; Waber, J. T. *International Tables for X-ray Crystallography*; Kynoch Press: Birmingham, U. K., 1974; Vol. IV.
(24) Becke, A. D. *J. Chem. Phys.* **1993**, *98*, 5648.
(25) Lee, C.; Yang, W.; Parr, R. *Phys. Rev. B* **1988**, *37*, 785.
(26) Frisch, M. J.; Trucks, G. W.; Schlegel, H. B.; Scuseria, G. E. M.; Robb, A.; Cheeseman, J. R.; Zakrzewski, V. G.; Montgomery, J. A.; Stratmann, R. E.; Burant, J. C.; Dapprich, S.; Millam, J. M.; Daniels, A. D.; Kudin, K. N.; Strain, M. C.; Farkas, O.; Tomasi, J.; Barone, V.; Cossi, M.; Cammi, R.; Mennucci, B.; Pomelli, C.; Adamo, C.; Clifford, S.; Ochterski, J.; Petersson, G. A.; Ayala, P. Y.; Cui, Q.; Morokuma, K.; Malick, D. K.; Rabuck, A. D.; Raghavachari, K.; Foresman, J. B.; Cioslowski, J.; Ortiz, J. V.; Stefanov, B. B.; Liu, G.; Liashenko, A.; Piskorz, P.; Komaromi, I.; Gomperts, R.; Martin, R. L.; Fox, D. J.; Keith, T.; Al-Laham, M. A.; Peng, C. Y.; Nanayakkara, A.; Gonzalez, C.; Challacombe, M.; Gill, P. M. W.; Johnson, B. G.; Chen, W.; Wong, M. W.; Andres, J. L.; Head-Gordon, M.; Replogle, E. S.; Pople, J. A. *Gaussian 98, Revision A.7*, Gaussian, Inc.: Pittsburgh, PA, 1998.
(27) (a) Dunning T. H.; Hay P. J. In *Modern Theoretical Chemistry*; Schaefer, H. F., III, Ed.; Plenum: New York, 1976; Vol. 3, p 1. (b) Hay, P. J.; Wadt, W. R. *J. Chem. Phys.* **1985**, *82*, 299.
(28) Hariharan, P. C.; Pople, J. A. *Theor. Chim. Acta* **1973**, *28*, 213.
(29) van Gisbergen, S. J. A.; Snijders, J. G.; Baerends, E. J. *J. Comput. Phys.* **1999**, *118*, 119.
(30) Casida, M. Time Dependent Density Functional Response Theory for Molecules. In *Recent Advances in Density Functional Methods*; Chong, D. P., Ed.; World Scientific: Singapore, 1995; Vol. 1, p 155.
(31) Fonseca Guerra, C.; Visser, O.; Snijders, J. G.; te Velde, G.; Baerends, E. J. In *Methods and Techniques for Computational Chemistry*, METECC-5, Clementi, E., Corongiu, G., Eds.; STEF: Cagliari; 1995, pp 305−395.
(32) van Leeuwen, R.; Baerends, E. J. *Phys. Rev. A* **1994**, *49*, 2421.
(33) ADF STO basis set database is available under http://www.scm.com.
(34) (a) Hoffmann, R.; Lipscomb, W. N. *J. Chem. Phys.* **1962**, *36*, 2872. (b) Hoffmann, R.; Lipscomb, W. N. *J. Chem. Phys.* **1962**, *37*, 3489.
(35) (a) Mealli, C.; Proserpio, D. M. *J. Chem. Educ.* **1990**, *67*, 399. (b) Mealli, C.; Ienco, A.; Proserpio, D. M., Eds.; CNR *Book of Abstracts of the XXXIII ICCC*; Florence, 1998; p 510.

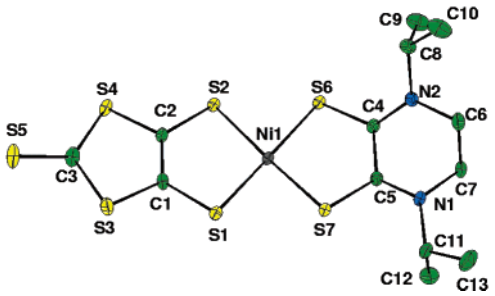

Figure 1. Complex [Ni(Pr$^i_2$pipdt)(dmit)], **1b**, with hydrogen atoms omitted for sake of clarity.

Table 2. Bond Lengths [Å] and Angles [deg] for [Ni(Pr$^i_2$pipdt)(dmit)]

Ni(1)−S(6)	2.1551(6)	Ni(1)−S(2)	2.1588(6)
Ni(1)−S(7)	2.1622(6)	Ni(1)−S(1)	2.1676(6)
S(1)−C(1)	1.735(2)	S(3)−C(3)	1.716(2)
S(2)−C(2)	1.732(2)	S(3)−C(1)	1.740(2)
S(4)−C(3)	1.724(2)	S(4)−C(2)	1.740(2)
S(5)−C(3)	1.665(2)	S(6)−C(4)	1.685(2)
S(7)−C(5)	1.697(2)	C(1)−C(2)	1.344(3)
C(4)−N(2)	1.327(3)	C(4)−C(5)	1.480(3)
C(5)−N(1)	1.324(3)	C(8)−N(2)	1.491(3)
C(11)−N(1)	1.486(3)		
S(6)−Ni(1)−S(2)	85.99(2)	S(6)−Ni(1)−S(7)	91.07(2)
S(2)−Ni(1)−S(7)	176.41(2)	S(6)−Ni(1)−S(1)	176.26(3)
S(2)−Ni(1)−S(1)	93.85(2)	S(7)−Ni(1)−S(1)	89.22(2)
C(1)−S(1)−Ni(1)	101.26(7)	C(2)−S(2)−Ni(1)	101.47(7)
C(3)−S(3)−C(1)	97.8(1)	C(3)−S(4)−C(2)	97.3(1)
C(4)−S(6)−Ni(1)	105.79(7)	C(5)−S(7)−Ni(1)	105.71(7)
C(2)−C(1)−S(1)	121.5(2)	C(2)−C(1)−S(3)	115.6(2)
S(1)−C(1)−S(3)	122.9(2)	C(1)−C(2)−S(2)	121.7(2)
S(5)−C(3)−S(3)	123.6(2)	N(2)−C(4)−C(5)	119.6(2)
C(5)−N(1)−C(7)	117.7(2)	C(5)−N(1)−C(11)	121.4(2)
C(7)−N(1)−C(11)	119.8(2)	C(4)−N(2)−C(6)	120.2(2)
C(4)−N(2)−C(8)	121.3(2)	C(6)−N(2)−C(8)	118.1(2)

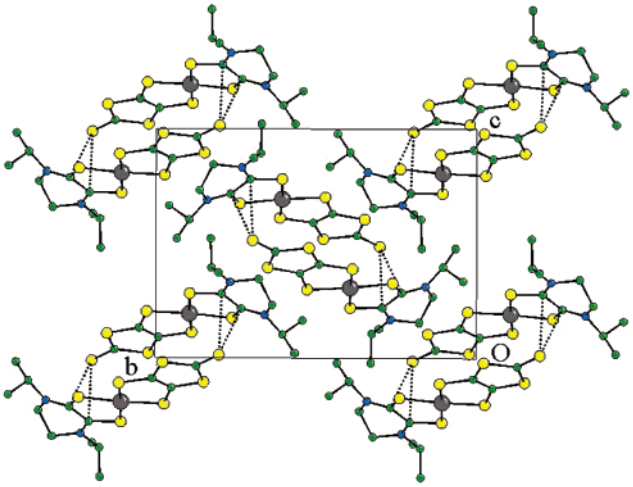

Figure 2. View of the crystal lattice of [Ni(Pr$^i_2$pipdt)(dmit)], **1b**, down the *a* axis of the unit cell.

Figure 1 shows the drawing of a discrete complex molecule of **1b**, where the metal atom is coordinated by the four S donors in a square-planar environment and four similar Ni−S distances (in the range 2.1551(6)−2.1676(6) Å). Selected bond distances and angles are given in Table 2.

Figure 2 shows that, in the crystal lattice, the complex units are almost parallel and head-to-tail with respect to each other. Relatively short contacts are observed between the terminal S-atom of dmit and the two carbon atoms of the C_2S_2 moiety of Pr$^i_2$pipdt belonging to the parallel molecule (3.42 and 3.34 Å, for S(5)−C(4)′ and S(5)−C(5)′, respectively).

The terminal six-membered ring of the ligand Pr$^i_2$pipdt is puckered as it contains a two-membered aliphatic chain. A puckering index of 0.97 (defined as $\Sigma_i\alpha_i/((n-2)\times 180)$, where α_i are the inner bond angles) and the torsion angle N(1)−C(6)−C(7)−N(2) of 54° confirm the nonplanarity of the ring. However, the sum of the three angles at each N atom (about 358°) indicates its essential sp^2 hybridization. Also, the torsion angles about the bonds N1−C7 and N2−C6 of only 10° suggest that the N p_π-lone pair is almost parallel to the C_2S_2 π system.

In Table 3, the geometric parameters of **1b** are conveniently compared with those of three other nickel-bis-dithiolene complexes presented in Scheme 2 and formed by a combination of the *push/pull* ligands. The compounds in question are [Ni(Me$_2$pipdt)(mnt)],[12] **2b′**,[13] [Ni(*c*Dod$_2$pipdt)-(mnt)] (*c*Dod = cyclododecyl), **2b‴**,[13] and [Ni(Pr$^i_2$timdt)-(dmit)], **3b**.[36]

Irrespective of the *push*/*pull* nature of the ligands, the four Ni−S coordination bonds are similar in all complexes (the range is restricted between 2.145(3) and 2.173(2)Å). This suggests that the Ni−S σ bonds are more or less equivalent and that Ni−S π interactions are of minor importance, if any. Conversely, a different electronic distribution at the ligands is highlighted by the comparison of the C−C and C−S bonds in the C_2S_2 units. The C−S distances are on the average 0.05 Å longer in dmit or mnt than in the ligands that feature N π-donors adjacent to the C_2S_2 grouping (Me$_2$-pipdt or R$_2$timdt). Consistent with the C−S π* and C−C π nature of the ligand's frontier MO (see Scheme 2), the C−C bond must be significantly longer in the electron poorer *push* than in the *pull* ligand. Differences up to 0.16 Å are observed, but, given the high standard deviations (>0.05 Å), the effect is likely overestimated. It is noteworthy that the thermal ellipsoids of the C_2S_2 carbon atoms of the *pull* ligand in the compounds **2b′** and **3b** are elongated toward each other, and, consequently, the C−C bond appears unrealistically short (1.29 Å for dmit in **3b**). The significant difference between C−C(X) and the C−C(Y) distances, in any case of Table 2, is indicative of localized π electron distribution (limiting VB structures A or C in Scheme 1). Accordingly, the structural data are indicative of *pull* character (dithiolate) for mnt and dmit ligands and of *push* character (dithione) for R$_2$pipdt and R$_2$timdt ones.

Electrochemical and Spectroscopic Studies. Electrochemical data for some of the compounds analyzed in this paper are presented in Table 4. In the complexes **1b** and **2b′**, which have in common one R$_2$pipdt ligand, the stepwise addition of two electrons requires progressively negative potentials; the analogous processes for the species **3b** and **4b** occur more easily (less negative potentials or even positive for the addition of the first electron to **4b**). By

(36) Bigoli, F.; Cassoux, P.; Deplano, P.; Mercuri, M. L.; Pellinghelli, M. A.; Pintus, G.; Serpe, A.; Trogu, E. F. *J. Chem. Soc., Dalton Trans.* **2000**, 4639−4644. Deplano, P.; Mercuri, M. L.; Pintus, G.; Trogu, E. F. *Comments Inorg. Chem.* **2001**, *22*, 353.

Table 3. Selected Distances (Å), within the $(C_2S_2)Ni(C_2S_2)$ Core, of Asymmetric Complexes Ni(X)(Y) Formed by a Combination of the *Push* (X) and *Pull* (Y) Ligands (Schemes 3 and 4)

[Ni(X)(Y)]	Ni−S(X)[a]	C−S(X)[a]	C−C(X)	Ni−S(Y)[a]	C−S(Y)[a]	C−C(Y)	ref
X = Pr^i_2pipdt; Y = dmit, **1b**	2.159(1)	1.691(2)	1.480(3)	2.159(1)	1.734(2)	1.344(3)	this work
X = Me_2pipdt; Y = mnt, **2b′**	2.162(2)	1.700(6)	1.433(3)	2.146(2)	1.735(6)	1.32(1)	12
X = *c*Dod_2pipdt; Y = mnt, **2b‴**	2.165 (3)	1.675(11)	1.50(2)	2.145(3)	1.732(12)	1.34(2)	13
X = Pr^i_2timdt; Y = dmit, **3b**	2.173(2)	1.694(6)	1.387(1)	2.147(2)	1.744(6)	1.29(1)	36

[a] Average value.

Table 4. Cyclic Voltammetric Data of [Ni(X)(Y)] (X = R_2pipdt and Pr^i_2timdt; Y = dmit and mnt)] Complexes

	E_a (V)[a] $M(X)(Y)^0 \rightarrow M(X)(Y)^+ + e^-$	$E^1_{1/2}$ (V) $M(X)(Y)^0 + e^- \rightleftharpoons M(X)(Y)^-$	$E^2_{1/2}$ (V) $M(X)(Y)^- + e^- \rightleftharpoons M(X)(Y)^{-2}$	HOMO/LUMO energies[b]
[Ni(Pr^i_2pipdt)(dmit)], **1b**	+0.590	−0.593[c]	−1.165[c]	−9.66/−8.74
[Ni(Me_2pipdt)(mnt)], **2b′**	+0.908	−0.527	−0.963	−10.61/−9.32
TBA[Ni(Pr^i_2timdt)(dmit)],[d] **3b**$^-$	+1.154	n.o.[e]	−0.402	−10.18/−9.49
[Ni(Pr^i_2timdt)(mnt)], **4b**	+1.160	+0.354	−0.307	−11.13/−10.16

[a] Irreversible. [b] Values (in eV) computed for the optimized geometries of the models **1a**−**4a** with the ADF package (see the theoretical section of the paper). [c] Quasi-reversible one-electron reduction. [d] Due to the low solubility of **3b**, its monoanionic salt, with tetrabutylammonium (TBA) as counterion, has been used as starting material for the electrochemical measurements. [e] Irreversible reduction observed at +0.234 V with a temperature of 25 °C.

anticipating some theoretical result, the computed energies of the LUMOs of the models **1a**−**4a** are reported in the last column of Table 4, together with those of the HOMOs.

The order of the LUMOs correlates well with that of the experimental $E^1_{1/2}$ and $E^2_{1/2}$ values and confirms that it is more difficult to add electrons in the species that contain the ligand R_2pipdt. This is because the two NH π-lone pairs, adjacent to the C_2S_2 moiety, destabilize significantly the empty level. Conversely, when the NH groups are inserted in a five-membered and delocalized ring (ligand R_2timdt in the complexes **3a** and **4a**), the LUMO lies lower (vide infra), as reflected by the corresponding $E^1_{1/2}$ and $E^2_{1/2}$ potentials. In particular, the positive one-electron reduction potential ($E^1_{1/2}$), measured for **4b**, is consistent with the lowest lying LUMO of the series (−10.16 eV for **4a**). In this case, the less strong *push* ligand R_2timdt accompanies the π-acceptor effects of the CN (*pull* ligand mnt) that partially stabilize the LUMO beside the HOMO.

The one-electron oxidation potentials (E_a) are relatable, not only to the energy of the HOMO, but also to the spin pairing energy of the electrons in this level. The potentials of the complexes **1b** and **2b′** are clearly less positive than those of **3b** and **4b** and the removal of one electron from the latter species is evidently a more difficult process. This seems consistent also with their lower lying HOMOs (although the order of **2a** and **3a** is inverted, their energies difference is not large). Again, by anticipating some argument of the theoretical section, the HOMO is mainly stabilized by the *pull* ligand, while the *push* ligand has a minor destabilizing effect. Thus the more difficult oxidation process for **2b′** vs. **1b** is consistent with the better stabilization of the HOMO induced by mnt vs. dmit. Finally, the complexes **3b** and **4b** exhibit the most positive oxidation potentials that cannot be only related to their lower HOMOs (the *push* ligand R_2timdt destabilizes the level less effectively than R_2-pipdt). Likely, the wide π-delocalization, which extends to the peripheries of these two totally planar complexes, affects the spin pairing energy of the electrons in the π-type HOMO.

Besides the electrochemical parameters, also the electronic spectra indicate a different behavior of the complexes **1** and **2** with respect to that of **3** and **4**. For instance, the molecular absorptivities (ϵ in Table 5) are significantly larger for the latter pair compounds, almost as if the species belonged to two different categories. However, this cannot be stated for the values of λ_{max} which are larger for the dmit complexes **1b** and **3b** than for the mnt analogues **2b′** and **4b**.

Table 5. Comparison of Electronic Spectra of the Complexes [Ni(X)(Y)] (X = R_2pipdt and Pr^i_2timdt; Y = dmit and mnt)

	λ_{max} (nm)	$\epsilon \times 10^{-3}$ (M^{-1} cm^{-1})
[Ni(Pr^i_2pipdt)(dmit)],[a] **1b**	965	10,9
[Ni(Me_2pipdt)(mnt)],[a] **2b′**	733	4,0
[Ni(Pr^i_2timdt)(dmit)],[b] **3b**	1056	39,0
[Ni(Pr^i_2timdt)(mnt)],[a] **4b**	883	24,1

[a] In $CHCl_3$. [b] In CS_2.

Finally, the FT-IR and Raman data provide some indication of the electron redistribution in the various complexes. By taking as reference the symmetric species $[Ni(mnt)_2]^{1-,2-}$ and $[Ni(dmit)_2]$,$^{1-,2-}$ the vibrational analyses show that the C═C stretch shifts to higher frequencies as the negative charge of the complex increases.[37,38] In fact, for the mnt redox derivatives, the corresponding peak of the monoanion occurs at 1435 cm^{-1} and that of the dianion at 1485 cm^{-1}. Analogously for the dmit species, the 1390 cm^{-1} value of the monoanion raises to 1435 cm^{-1} in the dianion. The mixed complex [Ni(Me_2pipdt)(mnt)] (**2b′**) exhibits a peak at 1492 cm^{-1}, while [Ni(Pr^i_2pipdt)(dmit)], **1b**, has a peak at 1440 cm^{-1}. These results suggest that the ligands mnt and dmit bear a formal charge close to −2 in the asymmetrical complexes with the Pr^i_2pipdt ligand. Conversely, when dmit and mnt are combined with Pr^i_2timdt (**3b** and **4b**, respectively), the C═C stretching peaks are found at frequencies similar to those of the respective symmetric monoanions (1425 and 1388 cm^{-1}, respectively). In conclusion the ligands dmit and mnt, when combined with Pr^i_2timdt, are still

(37) Schläpfer, C. W.; Nakamoto, K. *Inorg. Chem.* **1975**, *14*, 1338. Wootton, J. L.; Zink, J. I. *J. Phys. Chem.* **1995**, *99*, 7251.
(38) Pokhodnya, K. I.; Faulmann, C.; Malfant, I.; Andreu-Solano, R.; Cassoux, P.; Mlayah, A.; Smirnov, D.; Leotin, J. *Synth. Met.* **1999**, *103*, 2016.

Table 6. Selected Bond Distances (Å) for the Models **1a**−**4a**

complex	H_2pipdt Ni−S[a]/ C−C/ C−S[a]	H_2timdt Ni−S[a]/ C−C/ C−S[a]	dmit Ni−S[a]/ C−C/ C−S[a]	mnt Ni−S[a]/ C−C/ C−S[a]
1a	2.24/ 1.47/ 1.70		2.22/ 1.38/ 1.73	
2a	2.25/ 1.46/ 1.69			2.19/ 1.38/ 1.74
3a		2.26/ 1.42/ 1.69	2.22/ 1.38/ 1.73	
4a		2.27/ 1.43/ 1.68		2.19/ 1.39/ 1.73

[a] Average value.

attributable *pull* character but their negative charge must be lower than when combined with the better *push* ligand R_2-pipdt.

In conclusion, the electrochemical and spectroscopic results suggest a significant separation of charges in **1b** and, especially, in **2b′**, which combines the best *push* and *pull* ligands, Me_2pipdt and mnt, respectively. The effect is evidently reduced in **4b** and **3b**, with the latter being closest to a symmetric and delocalized distribution of the electron density.

Theoretical Approach. Optimization of the Geometries and Analysis of the Electronic Structures. To relate structure and properties, we have first optimized the geometries of the four complexes in Scheme 4 after replacing R substituents with H atoms. To this aim, Gaussian98 calculations at the DFT/B3LYP level were carried out for the closed shell models of [Ni(H_2pipdt)(dmit)], **1a**, [Ni(H_2pipdt)(mnt)], **2a**, [Ni(H_2timdt)(dmit)], **3a**, and [Ni(H_2timdt)(mnt)], **4a**. Subsequently, the optimized geometries were used to calculate the first excited states (as single points) as well as the first hyperpolarizability tensors. For the latter purpose, the ADF package (LB94 potential) was used. Table 6 presents a selection of the optimized distances in the four complexes, grouped for each ligand.

Although the geometry of the models **3a** and **4a** has been estimated by other authors with higher accuracy,[8] our coherent set of data allows meaningful comparisons in the series. In general, our calculations overestimate the Ni−S bonds by about 0.05−0.08 Å. Such a shortcoming was also reported for symmetric nickel dithiolenes (i.e., [Ni(H_2-C_2S_2)$_2$)]),[6b] while a slightly better agreement with the experiment (Δ = 0.03 Å) was found for the species [Ni(*o*-$C_6H_4S_2$)$_2$] by Bachler et al..[7] Finally, Lelj et al. underlined a similar incongruence for their systematic modeling of the symmetric complexes [M(H_2timdt)$_2$] and [M(H_2dmit)$_2$], M = Ni, Pd, Pt, when using the B3LYP/LAN2DZ model chemistry.[6d] Recently, the latter authors used a combination of the ADF/ZORA IV and V basis sets and obtained a rather satisfactory response for the M−S distances.[8] Irrespective of the latter problem, the present computational trend clearly indicates that the Ni−S distances are longer for the coordination of the H_2pipdt and H_2timdt than for that of the dmit and mnt ligands (2.26 and 2.24 Å vs. 2.22 and 2.19 Å, respectively). This suggests that a percentage of Ni═S double bond character associates with the ligands which adopt a larger dithiolate character, mnt in particular. Conversely, in the facing dithione ligand (see Scheme 1), the double bond character is more localized at the C═S bonds. In fact, the corresponding distances in the H_2pipdt and H_2timdt are shorter than those in dmit and mnt (1.69 and 1.68 Å vs. 1.73 and 1.73 Å, respectively). The relation is reverse for the intermediate C−C bond (1.46 and 1.42 Å vs. 1.38 and 1.38 Å, respectively). For the latter, the corresponding experimental parameters are not equally conclusive due to the significant thermal motion that affects the carbon atoms. For the ligands H_2timdt, dmit, and mnt, the computed C−C bond is up to 0.1 Å larger than the experimental one, while a relatively better agreement is found only for H_2pipdt (compare the values of 1.48 and 1.47 Å obtained for **1b** and **1a** with those of 1.43 and 1.46 Å determined for **2b′** and **2a**, respectively). In conclusion, the analysis of the geometric parameters agrees with the experimental Raman indication of a more negative charge in the dmit and mnt (dithiolates) with respect to that of the H_2pipdt and H_2timdt (dithiones).

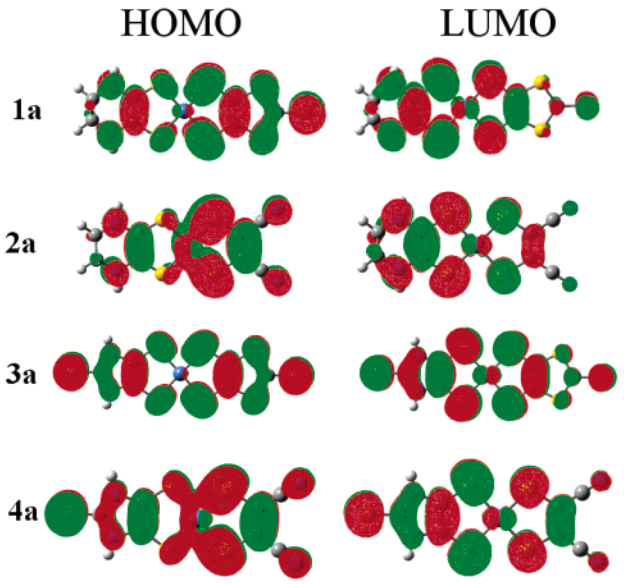

Figure 3. HOMO and LUMO of the models **1a**−**4a**.

Qualitative aspects of the frontier MOs provide useful information about the perturbations induced by the different terminal environments at the (C_2S_2)Ni(C_2S_2) core. Similarly to symmetric complexes (Scheme 2), the HOMOs and the LUMOs of the models **1a**−**4a** (Figure 3) are still ***ip*** and ***oop*** combinations of the critical C_2S_2 frontier π-orbital but the atomic contributions are now unbalanced, particularly when the ligand H_2pipdt is present. In fact, the greater weight of the latter in the LUMO is evident from the comparison of the HOMO and LUMO drawings of **1a** and **2a**. Another important aspect, that will be focused on later, is the scarce contribution of the terminal CS_3 moiety of dmit to the LUMO of both complexes **1a** and **3a**.

The compositional trends may be interpreted with the help of the qualitative diagrams in Figure 4. The latter are constructed from EHMO calculations,[34,35] which provide MO

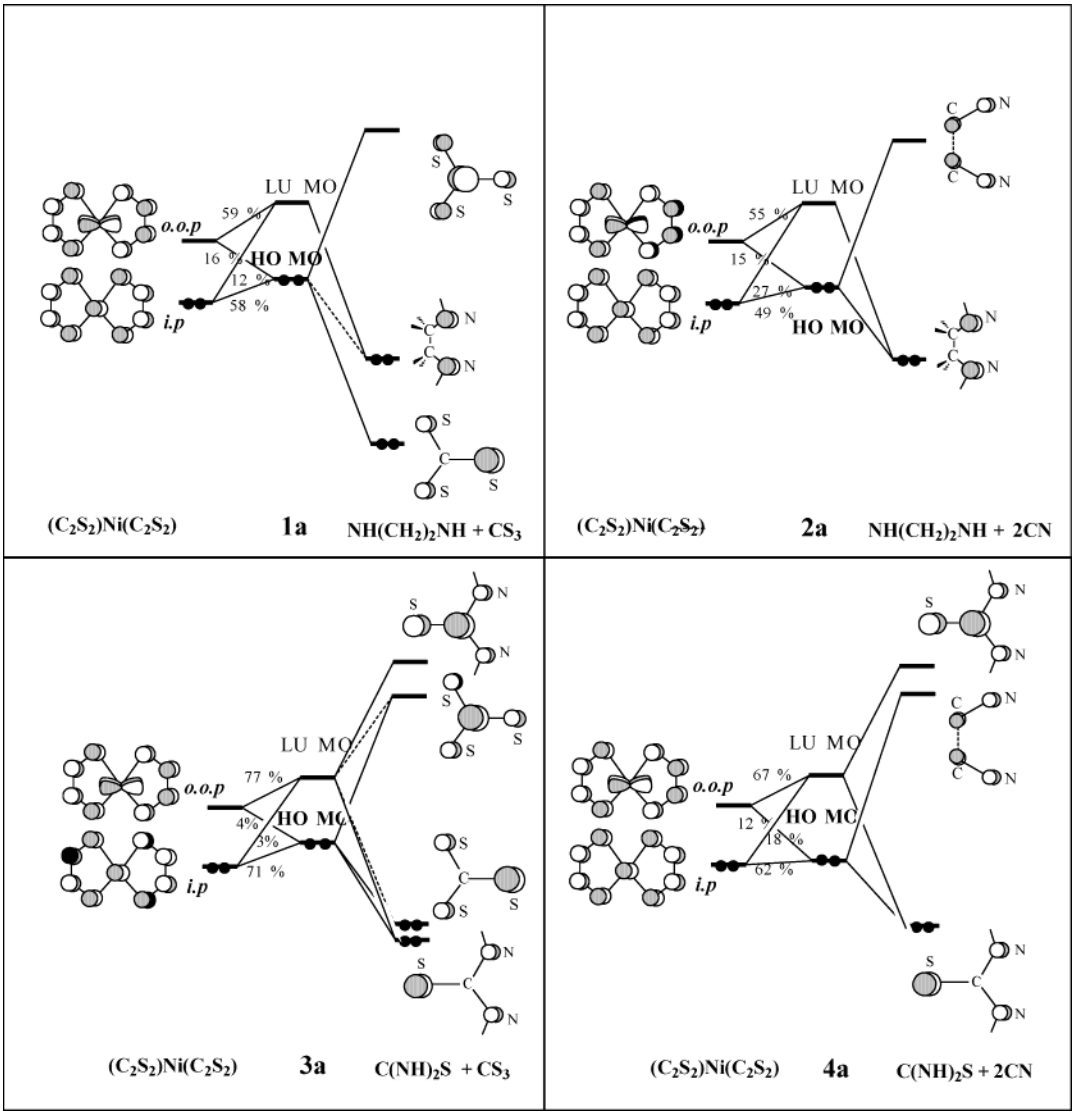

Figure 4. Qualitative interaction diagrams showing the perturbation of the left and right different environments over the $(C_2S_2)Ni(C_2S_2)$ core.

pictures and HOMO−LUMO gaps rather consistent with those of the DFT method. The FMOs of the central unit $(C_2S_2)Ni(C_2S_2)$ are reported at the left side of each diagram, while those of the terminal groupings are at the right sides. The latter have π−donor or π−acceptor capabilities, which perturb the MO picture of the core in a more or less asymmetric fashion and induce the mixing of the ***ip*** and ***oop*** frontier levels, which is also an important parameter for the presence or absence of NLO properties.[14,39] For this reason and in agreement with the pictures of Figure 4, all the HOMOs feature a contribution of a d_π metal orbital, which was originally consistent only with the ***oop*** combination of the core. Obviously, the inter-level mixing is minimum ($\leq$ 4%) for the complex **3a**, which is almost symmetric since the ligands H_2timdt and dmit differ only for carrying a pair of NH or S units.

Let's consider first the most antithetic roles of the ligands mnt and H_2pipdt. From both Figures 3 and 4, it is evident that the two CN groups of mnt act as π−acceptors toward the attached C_2S_2 unit and stabilize the $(C_2S_2)Ni(C_2S_2)$ ***ip*** combination, which becomes the HOMO of the uncharged complex. Conversely, the ligand H_2pipdt affects the ***oop*** combination of the core since the NH filled $p_{\pi-}$ orbitals (practically orthogonal to the plane of the core) behave as donors to the adjacent C_2S_2 unit and raise the LUMO but also have a minor destabilizing effect on the HOMO. In conclusion, the combination of the ligands mnt and H_2pipdt (complex **2a**) determines the largest observed HOMO−LUMO gap [$\Delta E = 1.30$ eV,[40] see Table 7]. For comparison, the gap in the π-unperturbed symmetric complex $(H_2C_2S_2)$-$Ni(H_2C_2S_2)$, is 0.99 eV.[40] Remarkably, the combination of the most effective *push* and *pull* ligands cause the greatest

(39) Marder, S. R.; Son, J. E.; Beratan, D. N.; Cheng, L.-T. *Science* **1991**, *252*, 103.

(40) For consistency with the other parameters introduced in eq 1, the HOMO and LUMO energies and the corresponding ΔE_{eg} values are those obtained from calculations carried out with the ADF package. In particular, the magnitudes are derived from single point calculations for the open shell singlet state by using the geometries optimized with Gaussian98. In fact, it is well-known that, for closed shell calculations, the energies of the virtual (empty) orbitals are less reliable than those of the doubly occupied levels. In any case, the order of frontier level energies and their differences are rather consistent in the two approaches.

Table 7. Computed and Experimental Molecular First Hyperpolarizability $\beta_{(z,z,z)}$ as Fully Determined with the ADF Package for the Models **1a**−**4a**[a]

complex	ground-state dipole moment μ_g	excited-state dipole moment μ_e	$\mu_e-\mu_g$	μ_{ge}^2	ΔE_{ge}[b] $1/\Delta E_{ge}^2$	$\beta_{(z,z,z)}$[c]	oscillator strengths[d]/ excitation energies[e]
[Ni(H_2pipdt)(dmit)], **1a**	11.8	9.0	−2.8	23.2	0.92 1.18	−73	0.11 (70%) / 1.22
[Ni(H_2pipdt)(mnt)], **2a**	19.5	16.5	−3.0	18.1	1.30 0.59	−28	0.10 (62%) / 1.46
[Ni(H_2timdt)(dmit)], **3a**	2.2	1.0	−1.2	28.4	0.69 2.1	−40	0.13 (76%) / 1.18
[Ni(H_2timdt)(mnt)], **4a**	11.6	9.8	−1.8	26.3	0.98 1.04	−5	0.14 (78%) / 1.36

[a] Also given are the various components [μ_g, μ_e, μ_{ge}^2, ΔE_{ge}] that appear in eq 1. The dipole moments are given in debye units, the energies are in eV, and the hyperpolarizabilities are in 10^{-30} esu units. [b] The discrepancy between the present ΔE_{ge} values and those derived from the HOMO−LUMO energies reported in Table 4 is due to the different computational approach (see footnote 40). [c] Value (in esu) computed with the ADF−RESPONSE module. [d] Computed value for the lowest optically allowed transition state. In parentheses, the percent of the HOMO−LUMO CT-contribution. [e] In eV.

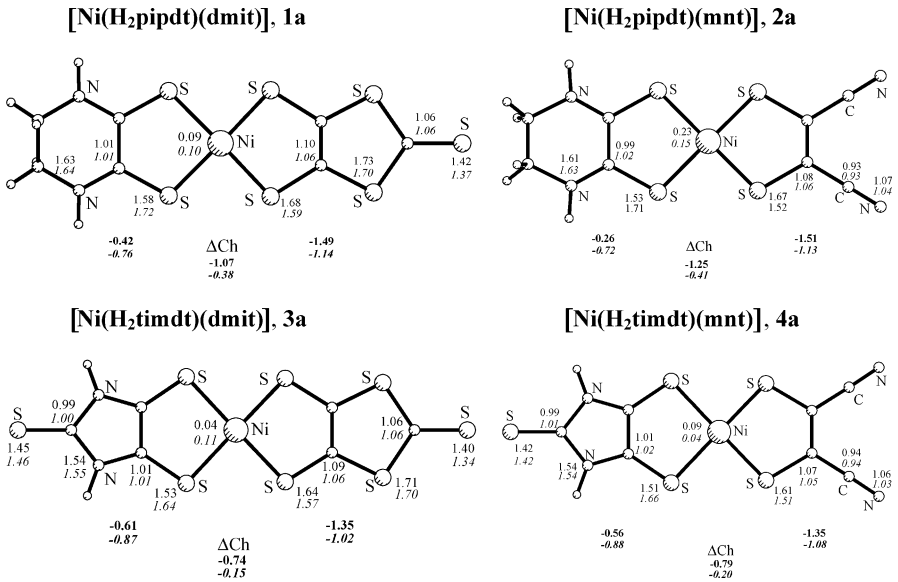

Figure 5. Computed π-electron populations of the atoms lying in the main plane of the complexes **1a**−**4a** for the ground and first excited (italics) states. Below each drawing, the π charge of each ligand is reported as well as the $\Delta_{Charges}$ for the two states. The latter were calculated by considering that the total π-electron population is 8 for the neutral H_2pipdt and mnt ligands, and 10 for the H_2timdt and dmit ones.

separation of charges (vide infra), hence the largest ground-state dipole moment (μ_g = 19.5 D).

Also, the ligand H_2timdt features two NH groups linked to the C_2S_2 unit but inserted in a five- rather than six-membered ring. This reduces the *push* character with respect to that of H_2pipdt, particularly as a consequence of the overall planarity and of the large π-delocalization which extends to the exocyclic C═S bond. Mainly, two π−combinations of the $(NH)_2CS$ unit perturb the frontier levels of the core (see the diagrams for **3a** and **4a** in Figure 4). The lower FMO acts as a donor toward the ***oop*** combination and destabilizes the LUMO but not as much as the ligand H_2pipdt. The higher π*-FMO barely interacts with the ***ip*** combination of the core because of a significant energy gap but it prevents the LUMO from raising too much in energy. In fact, the level is the lowest in the series (see Table 4). This is also true for the HOMO because the stabilizing effect of mnt is not equally counterbalanced by a strong π donor power such as that of H_2pipdt in **2a**. In any case, the HOMO−LUMO gap of **4a** (0.98 eV)[40] is the second in the series (see Table 7).

Next, we address the role of the terminal CS_3 unit in the ligand dmit. In principle its perturbative effect should not be very dissimilar from that of the $(NH)_2CS$ unit in the ligand H_2timdt. Indeed, the complex [Ni(H_2timdt)(dmit)], **3a**, is close to being symmetric as inferred by the small dipole moment, computed to be 2.2 D at the ground state. Still, the latter nonzero value suggests an asymmetric distribution of the π-charges (see later Figure 5), which is consistent with the distinctive *push* and *pull* characters of the two ligands. The interaction diagram of **3a** in Figure 4 helps to interpret the respective roles. The lower frontier π-FMOs of the CS_3 and $(NH)_2CS$ units have very similar shapes and energies and equally contribute to raising the LUMO of the complex. However, Figure 3 shows that the contribution of CS_3 to the LUMO is rather small, as it is partially canceled by its higher π*-FMO. However the latter, which lies about 0.7 eV lower than its $(NH)_2CS$ analogue, plays a prevailing π-acceptor role toward the ***ip*** combination of the core, which cannot be exerted by $(NH)_2CS$. On the basis of the previous considerations, it can be understood why the HOMO−LUMO gap of **3a** is the smallest in the series (0.69 eV), a fact which will ultimately influence the NLO properties of the species.[40]

The *pull* character of dmit is confirmed when this is combined with the strong π-donor ligand H_2pipdt (complex **1a**). The p_π-lone pairs of the latter raise the LUMO at an

energy higher than that of **2a** (where the CN π*-orbitals play some stabilizing effect) while the contribution of CS_3 to the level is minimum. On the other hand, the CS_3 π*-FMO stabilizes the HOMO but not as much as in **3a** due to the opposite effect of the π-donor ligand H_2pipdt. Eventually, the HOMO−LUMO gap (ΔE of 0.92 eV)[40] is only greater than that of **3a** but **1a** is remarkably the best NLO chromophore in the series!

Computational Analysis of the NLO Properties. The NLO behavior and the molecular first hyperpolarizability β, in particular, have been quantitatively evaluated for all the studied species by using the module RESPONSE[29] of the ADF package.[30] The emerging trend is satisfactorily consistent with that of the measured βs on the complexes **1b**, **2b″**, **4b** (−135, −37, $\approx 0 \times 10^{-30}$ esu, respectively), namely **1a** > **2a** > **4a** (absolute values, see Table 7). Importantly, nonzero NLO properties are predicted for the complex **3a**, which could not be detected experimentally. In fact, the computed $\beta_{(z,z,z)}$ value of -40×10^{-30}esu is only smaller than that of **1a** (-73×10^{-30}esu). The result is somewhat surprising since, on the basis of the similar electrochemical and spectroscopic behavior within the pairs **1b**−**2b** and **3b**−**4b**, almost null first molecular hyperpolarizability could be reasonably expected for **3a**, analogously to the case of **4a**.

To gain some hint on the origin of the various NLO responses, the components of the two-level formula (equation 1) have been separately evaluated. The approach is justified by the asymmetric π−delocalization of the complexes **1a**−**4a**, which is similar to that of many NLO organic systems with an aromatic core.[14] In these cases, the first optically allowed excited state (fixed by all the possible transitions between filled and empty levels complying with the given symmetry) is dominated by the HOMO−LUMO charge-transfer term (CT). Marder et al.[39] first addressed the interrelations among μ_{ge}^2, $\mu_e - \mu_g$ (= $\Delta\mu$) and $1/\Delta E_{ge}^2$ on the basis of EHMO calculations, and similar conclusions were reached by Yoshimura.[41−43] In our case, μ_g and μ_e are easily obtained from the single point calculations of the diamagnetic ground state and of the singlet excited state with two unpaired electrons (ADF package with the Gaussian optimized geometry). Analogously, the ΔE_{ge} term is readily available from the evaluation of the HOMO and LUMO energies.[40] Less straightforward is the derivation of the transition dipole moment μ_{ge} to be used in the eq 1. In fact, the output of the ADF−RESPONSE module provides the global magnitude relative to all the possible transitions of the given, optically allowed, excited state but not the matrix elements for the single transitions, in particular the HOMO−LUMO one. Thus an estimation of β from eq 1, by using the available μ_{ge}^2 value, is justified only by the high percentage with which the lowest transition contributes to the oscillator strength (between 62% and 78% for the species **1a**−**4a**, as reported in last column of Table 7).

Due to the forced approximations, the order of the β values (**1a** ≈ **3a** > **4a** ≈ **2a**), estimated by applying eq 1, does not match that from measurements or calculations with the TD_DFT method. However, the analysis of the basic components helps to clarify several aspects. In particular, there is a good rationale for the evident difference between **1a** and **4a**, while the quasi symmetric species **3a** is predicted to have an unexpectedly large NLO response.

As expected, the negative sign of β is imposed by the difference $\mu_e - \mu_g$, i.e., the charge separation is smaller in the excited than in the ground state. $\Delta\mu$ must be rigorously zero for symmetric complexes and should be also small for a combination of strong π donors and acceptors that impose large and almost equivalent dipole moments in the two states.[39] In our case, the quasi-symmetric species **3a** has the smallest $\Delta\mu$ value (= −1.2 D), with the μ_e and μ_g terms both being small. By increasing the strength of the *pull* ligand (mnt in place of dmit, as in **4a**), the separation of charges varies significantly (the μ_g and μ_e values become 11.6 and 9.8 D, respectively) but the effect is not large on $\Delta\mu$ (= −1.8 D). More pronounced are the effects of the better *push* ligand H_2pipdt, which is present in **1a** and **2a**, with $\Delta\mu$ values of −2.8 and −3.0 D, respectively. In the former case, the μ_g and μ_e components are similar to those of **4a** (11.8 and 9.0 D, respectively), probably because the effect of the better π-donor is counterbalanced by that of the poorer π-acceptor (dmit < mnt). By the same token, the combination of the most perturbing *push*/*pull* substituents (ligands H_2pipdt and mnt, respectively) confers to **2a** the largest μ_g and μ_e values (19.5 and 16.5 D) and the most pronounced $\Delta\mu$ (= −3.0 D).

Figure 5, which reports the populations of the p_π-atomic orbitals in the ground and excited (italics) states, is useful to correlate the π-electron distribution with the various dipole moments and their differences. In all cases, the *pull* character of the right side ligand is consistent with its more negative π-charge (dithiolate) with respect to the *push* ligand (dithione) at the left side. Although the charges are more equally distributed in the excited state, the trend is far from vanishing or being inverted. Consistently with the estimated $\Delta\mu$s, the $\Delta Ch_g - \Delta Ch_e$ difference is larger for compounds **1a** (−0.69) and **2a** (−0.84) than for **3a** (−0.59) and **4a** (−0.59). This suggests that the *push* power of H_2pipdt (vs. that of H_2timdt) is more effective than the *pull* power of mnt (vs. that of dmit).

Another interesting aspect is that, from the ground to the excited state, the p_π-orbital populations change more significantly at the core than at the peripheral atoms. The evident exception is the terminal S atom of dmit that, independently from the nature of the facing ligand, is significantly less populated in the excited state (by 0.05−0.06 electrons). Recall in this respect that the low lying CS_3 π* level confers to dmit π-acceptor capabilities not available to H_2timdt (see Figure 4 and its interpretation). Consistently, the two dmit complexes **1a** and **3a** carry a CS_3 contribution larger in the HOMO than in the LUMO as confirmed by the respective drawings presented in Figure 3. Thus, the unexpectedly nonnull β value of **3a** (a quasi symmetric complex) may have its underpinnings in the qualitative MO similarity with **1a**, which features the largest first hyperpolarizability of the series.

(41) Yoshimura, T. *Appl. Phys. Lett.* **1989**, *55*, 534.
(42) Yoshimura, T. *Phys. Rev. B* **1989**, *40*, 6292.
(43) Yoshimura, T. *Mol. Cryst. Liq. Cryst.* **1990**, *182*, 43.

The parameter μ_{ge}^2 varies inversely to $\Delta\mu$, the trend being evident from the values reported in Table 7. The computed μ_{ge}^2 values are expected to be proportional to the molecular absorptivities ϵ and, indeed, follow the order **2a** < **1a** < **4a** < **3a**. Recall, in this respect, that the experimental ϵ values (see Table 5) were drastically larger for the latter two complexes almost as if they belonged to a different category. According to Marder et al.,[39] analogous ordering should be expected for the parameters $1/\Delta E_{ge}^2$.[39] Indeed, the two extreme values are those of **3a** and **2a** (2.1 and 0.59 eV^{-2}, respectively). For the intermediate compounds, the magnitudes are similar although in a reverse order with respect to that of squared transition dipole moments (1.18 and 1.04 eV^{-2}, for **1a** and **4a**, respectively).

The major drawback for a correct application of the two-level formula is the unavailability of the single μ_{ge}^2 matrix elements for the HOMO−LUMO transitions. As mentioned, the latter elements represent a percentage of the oscillator strength, which is significantly smaller in **1a** and **2a** than in **3a** and **4a**. Thus, the introduction of the global μ_{ge}^2 values in the two-level expression 1 likely overestimates the βs of the latter pair of compounds (see Table 7). On the other hand, the analysis of the components justifies well the larger β of **1a** with respect to that of **2a**, although the latter features the greatest separation of charges. In fact, the difference is clearly attributable to the smaller ΔE and the larger μ_{ge}^2 values (0.92 vs. 1.30 eV and 23.2 vs. 18.1 D^2, for **1a** vs. **2a** respectively). Notice in particular the good correlation of the μ_{ge}^2 magnitudes with experimental molecular absorptivities of **1a** and **2a** (10.9×10^3 and 4.0×10^3 $M^{-1}cm^{-1}$, respectively).

Analogous arguments account for the order of the estimated βs of **3a** and **4a**. As anticipated by the experimental ϵ values (39.0×10^3 and 24.1×10^3 $M^{-1}cm^{-1}$, respectively), the large μ_{ge}^2 magnitudes (28.4 and 26.3 D^2, respectively) should determine large βs. For the **3a**, in particular, the smallest ΔE value (0.69 eV) is another factor favoring β, which is only counterbalanced by the small $\Delta\mu$ (−1.2 D). In contrast, the quasi-null NLO properties of **4a** (as calculated by the ADF−RESPONSE module and experimentally measured) are somewhat contradicted by the two level formula. Although it cannot be excluded that the $\Delta\mu$ and/or the $1/\Delta E_{ge}^2$ components are ill-estimated in this case, the usage of the global transition dipole moment in place of its HOMO−LUMO component is particularly overestimated in this case.

Despite some drawbacks, the two-level formula and its components illustrate many interesting aspects relative to the spectroscopic and NLO behaviors of the four complexes investigated. The better *push* ligand (R_2pipdt in **1a** and **2a**) destabilizes significantly the LUMO and favors the separation of charges (higher dipole moments of the ground and exited states and larger $\Delta\mu$s). However, the transition dipole moments of **1a** and **2a** (consistently with the experimental ϵ values) are clearly smaller than those induced by the other *push* ligand H_2timdt, and, by themselves, do not justify well the different extent of the NLO properties. At this point, the role of the *pull* ligands mnt and dmit must be underlined, and, especially, that of the latter in **1a** and **3a**. In fact, the most remarkable NLO response is exhibited by the former complex, while that of **3a** is also unexpectedly large. As we have underlined above, the way by which the two CS_3 π and π*-levels mix in the frontier MOs is peculiar. As a consequence, not only the HOMO−LUMO gaps are small and favor larger βs but also the distribution of the electrons in the two critical levels is moderately asymmetric to cause sufficiently high transition dipole moments.

Conclusions and Perspectives

Structural, spectroscopic studies and theoretical calculations have been performed for selected uncharged bis-dithiolene nickel complexes that have been experimentally ascertained to feature second-order NLO properties. For one of the four cases investigated (complex **3a**), the first molecular hyperpolarizability (experimentally not available) has been computationally predicted. The study, besides reporting the crystal structure of [Ni(Pr^i_2pipdt)(dmit)] as well as a detailed comparison with the available ones, has been aimed to find the relationships between the structural and electronic features of the four compounds. To this purpose, structural optimizations of model compounds have been systematically carried out, and, for each of the latter, the molecular first hyperpolarizabilities have been computed by using the ADF−RESPONSE module. Additionally, the simplest two-level model has been adopted to interpret the electronic origin of the NLO properties. As expected, the latter depends on a number of factors which have been all systematically pointed out from both the quantitative (single components of the two-level expression 1) and qualitative points of view. In particular, perturbation theory arguments have been exploited to account for the nature of the critical frontier MOs and the effect of the asymmetric environment about the central core. Thus, the analysis accounts for the various NLO responses in terms of the important components $\Delta\mu$, μ_{ge}^2, and $1/\Delta E_{ge}^2$. Interestingly, the remarkable first molecular hyperpolarizability predicted for the quasi-symmetric complex **3a**, has highlighted the unique role of ligand dmit in perturbing the electron distribution of the (C_2S_2)Ni-(C_2S_2) core and in inducing major differences between the ground and excited states. Its usage will be privileged in our continuing research on this type of NLO-phores.

Acknowledgment. P.D. thanks Università di Cagliari for financial support and INSTM for providing computing time at CINECA. Thanks are also due to Dr. M. Placidi, Jobin Yvon srl, for running the Raman spectra. A.I. and C.M. are grateful for the computing time provided by CINECA under the agreement with the CNR. Work at Universitá di Cagliari and LCC-CNRS, Toulouse, is supported by the European COST Action D14-003.

Supporting Information Available: X-ray crystallographic file in CIF format for **1b**. This material is available free of charge via the Internet at http://pubs.acs.org. A collection of Cartesian coordinates and total energies for all of the optimized molecules is available from C.M. upon request.

IC0496469